Single-Molecule Measurement of the Stiffness of the Rigor Myosin Head

Alexandre Lewalle,* Walter Steffen,† Olivia Stevenson,* Zhenqian Ouyang,* and John Sleep*
*Randall Division, King's College London, London, United Kingdom; and †Medical School Hannover, Hanover, Germany

ABSTRACT The force-extension curve of single myosin subfragment-1 molecules, interacting in the rigor state with an actin filament, has been investigated at low [ATP] by applying a slow triangle-wave movement to the optical traps holding a bead-actin-bead dumbbell. In combination with a measurement of the overall stiffness of the dumbbell, this allowed characterization of the three extensible elements, the actin-bead links and the myosin. Simultaneously, another method, based on an analysis of bead position covariance, gave satisfactory agreement. The mean covariance-based estimate for the myosin stiffness was 1.79 pN/nm (SD = 0.7 pN/nm; SE = 0.06 pN/nm (n = 166 myosin molecules)), consistent with a recent report (1.7 pN/nm) from rabbit muscle fibers. In the triangle-wave protocol, the motion of the trapped beads during interactions was linear within experimental error over the physiological range of force applied to myosin (±10 pN), consistent with a Hookean model; any nonlinear terms could not be characterized. Bound states subjected to forces that resisted the working stroke (i.e., positive forces) detached at a significantly lower force than when subjected to negative forces, which is indicative of a strain-dependent dissociation rate.

INTRODUCTION

In the basic form of the swinging cross-bridge model of muscle contraction, the myosin cross-bridge performs work by a structural change that tensions an elastic element, the energy being released during subsequent shortening of the muscle fiber. The amount of energy stored is governed by the stiffness of the elastic element, and since its importance was first appreciated (1), this model has been intensively investigated in muscle fibers. Although it is conceptually simple to measure the stiffness of a muscle fiber by applying a small length change and determining the increase in tension, in practice there are technical challenges, one of which is to compensate for the effects of other elastic elements acting in series with the cross-bridges. The first evidence for the significant compliance of actin filaments came from an experiment in which a single filament of actin was stretched between microneedles (2), but the values obtained were confirmed shortly afterward in muscle fibers by studying the axial x-ray reflection (2.7 nm) arising from the actin filaments (3,4). The myosin reflections were also observed to change in a manner consistent with myosin filament extension. Since that time, the application of high-resolution (both temporal and spatial) mechanical methods (5), in combination with high-resolution x-ray methods, has allowed a very detailed analysis of the significance of filament compliance. Myosin cross-bridges account for only ~40% of the compliance of a fiber, so that to reduce the isometric tension to zero requires interfilament sliding of only about 1.7 nm (6,7). This distance is in striking contrast to the estimates of the working stroke, which have remained broadly constant at ~10 nm despite significant refinement in technology, and because of this apparent mismatch it is unlikely that the working stroke can take place in a single step (7). The comparison of the stiffness of an isometric fiber and a rigor fiber provides an estimate of the fraction of attached heads during isometric contraction of 30–40%, a figure that, in combination with the value 1.7 nm, provides an estimate for the stiffness of a myosin cross-bridge of ~3 pN/nm. This high stiffness is the cause of the mismatch. This value is considerably higher than that reported in the most recent detailed study of the myosin stiffness by single-molecule methods (0.7 pN/nm (8)), although intermediate values have been reported as by-products of other investigations, for example, 1–2 pN/nm (9), 1.1 pN/nm (10), and 1.3 pN/nm (11). The single-molecule methods already seem out of line with fiber studies with respect to the size of the working stroke (~5 nm cf. 10 nm), and it seemed desirable to investigate whether this discrepancy really did extend to the myosin stiffness or whether a more detailed investigation might close the gap. After this work was completed, a new value (1.7 pN/nm) for the stiffness of myosin heads in rabbit fibers was reported that substantially reduced this discrepancy (12).

In this study, we measured the stiffness of single myosin cross-bridges, which avoided the difficulty faced by muscle fiber physiologists of having to estimate the fraction of interacting cross-bridges, but shared with them the need to correct for series compliant elements. We used a new ''ramp'' method that provides estimates of the stiffness values for both the myosin and the two actin-bead links. The results were directly compared with those of Smith et al. (9), who employed an experimentally very convenient method for measuring the same parameters. To date, single-molecule methods have only been used to explore the force-extension curve either under mechanical conditions that are not well defined (13) or, alternatively, over a restricted range of strain. The methods of Mehta et al. (14) and Smith et al. (9) mea-

Submitted August 8, 2007, and accepted for publication November 7, 2007.

Address reprint requests to John Sleep, Randall Division, King's College London, London SE1 1UL, UK. E-mail: john.sleep@kcl.ac.uk.

Editor: E. Michael Ostap.

0006-3495/08/03/2160/10 $2.00

doi: 10.1529/biophysj.107.119396

sured the response to thermal motion, whereas Veigel et al. (8) looked at a range of forces up to ~10% of the in vivo force borne by a myosin head. The ramp method allows exploration of the force-extension curve of the myosin head over the full physiological range of forces (±10 pN).

Another characteristic of the actomyosin cross-bridge is the extent to which force accelerates dissociation. In the case of stretching muscle, this has been investigated in some detail by Lombardi and Piazzesi (15). Such mechanical breakage may also occur during shortening of muscle, although inferences made from such a process are more model-dependent than in the stretching case. A characterization of the effect of strain on dissociation comes naturally out of our ramp method of assessing cross-bridge stiffness.

METHODS

The bead-actin-bead dumbbell

In the standard ''dumbbell'' method of investigating the properties of single molecules of myosin (16,17), the myosin head is bound to a glass bead that is fixed on the microscope coverslip, and this head is allowed to interact with an actin filament that is stretched between two micron-sized, optically trapped latex beads. The motion of the actin filament is not directly observable, and information must be inferred from the position of the trapped beads.

The stiffness of the actin-bead links k_{L1} and k_{L2} is dependent on the tension in the filament in a nonlinear manner (18), but although the links become progressively stiffer as the tension is increased, they behave in a Hookean manner for small perturbations, allowing the system to be modeled as an assembly of linear springs (see Fig. 1). The actin filament (of length ~6 μm) is much stiffer than a single cross-bridge (3), and its compliance is negligible in our single-molecule experiments. In contrast, in a sarcomere, many cross-bridges are interacting with each actin filament and the total stiffness of these bound cross-bridges is similar to that of the filament. In consequence, the actin compliance cannot be neglected in fiber experiments.

Under normal experimental conditions, the actin-bead link stiffnesses (see Fig. 1) are an order of magnitude larger than the trap stiffnesses k_1 and k_2 (~0.06 pN/nm), and when the actin is not attached to the myosin, the motion of the dumbbell approximates that of a rigid body. The stiffness of the two traps is equalized while the dumbbell is slack, and then the combined stiffness of the two traps is measured from the thermal fluctuation during the experiment to allow for the small decrease in the effective stiffness as the beads are pulled from the center of the trap (19).

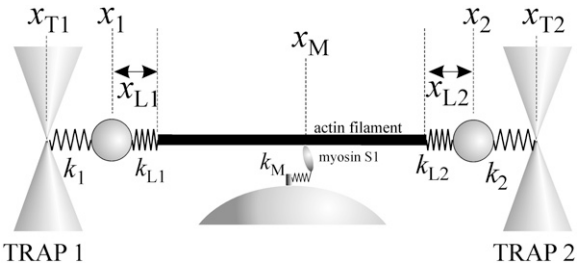

FIGURE 1 Compliant elements in a dumbbell experiment: trap stiffnesses k_1 and k_2; actin-bead link stiffnesses k_{L1} and k_{L2}; and myosin head stiffness k_M. Labels indicate trap positions x_{T1} and x_{T2} and bead positions x_1 and x_2 measured relative to an arbitrary origin. The extensions of the actin-bead links and the myosin spring are x_{L1}, x_{L2}, and x_M.

The ramp method

The main experiment described in this article involves applying a large-amplitude (0.2–0.5 μm) triangular wave of exactly equal amplitude to both optical traps while allowing interactions between the actin and myosin to occur during the upward and downward ramps. For the force-extension curve to be characterized over the physiological range, an appropriate combination of event duration (controlled by [ATP]) and ramp velocity must be chosen, and for rabbit myosin at ~22°C a ramp velocity of 400 nm s^{-1} with an [ATP] of 2 μM was found to be appropriate. At this velocity, the viscous drag on the 1-μm beads was only 0.004 pN, very much lower than the forces imposed by the ramp during binding events.

When the dumbbell is not bound to myosin, the beads follow the motion of the traps and, when the dumbbell is bound, the myosin exerts a restraining force on the dumbbell, making the beads move more slowly than the traps. Events for analysis were detected by subtracting the background triangular pattern from the bead signals and then locating the time periods in which the bead signals departed beyond the range of thermal noise.

The motion of the two beads in a given bound state depends on the stiffnesses of the myosin and those of each of the actin-bead links. A representative record of the motion of the two beads during an upward ramp of the triangular wave is shown in Fig. 2. It is immediately clear that the actin link with bead 2 is less stiff than that with bead 1 because, first, bead 2 is slowed significantly less than bead 1 and, second, the variance of position of bead 2 in the bound state is higher than that of bead 1. The linearity of the bead motion in the bound state supports the assumption, made in the model (Fig. 1), that all the elastic elements behave like Hookean springs over the applied range of forces. In view of the linearity, each event can be characterized in terms of the two measurable quantities R_1 and R_2 (see Fig. 2):

$$R_i = \frac{[dx_i/dt]_{bound}}{[dx_i/dt]_{unbound}}, \quad i = 1, 2. \tag{1}$$

To extract the three unknown parameters, the myosin stiffness, k_M, and the actin-bead link stiffnesses, k_{L1} and k_{L2}, it is necessary to make a third measurement of the combined series stiffness, k_L, of the two actin-bead links:

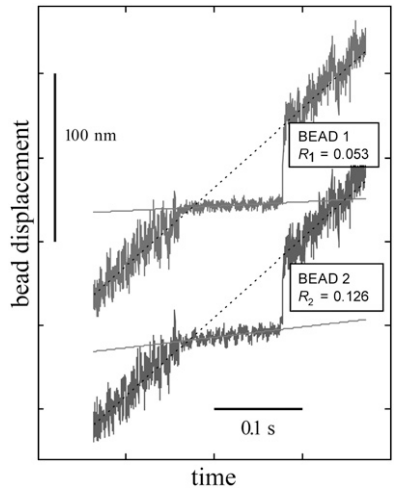

FIGURE 2 Bead displacement during a slow ramp of both traps. The trap positions were moved past the myosin at a rate of 0.4 μm/s, allowing the myosin to interact. The large stiffness of myosin and the bead-actin links, compared with that of the traps, hinders the motion of the beads, and for each bead, this effect is characterized by the ratio of bound to unbound velocities, R. In this example, $R_1 < R_2$, because the bead 1-actin link is stiffer than the bead 2-actin link. For the same reason, the variance of bead position 1 (3.1 nm^2) is less than that of bead position 2 (6.4 nm^2).

$$k_L = \frac{k_{L1}k_{L2}}{(k_{L1} + k_{L2})}. \quad (2)$$

A force-extension curve can be obtained for each bound period by calculating, as a function of the trap displacements, the total force, F_M, exerted on the beads by the traps, and the corresponding extension, x_M, of the myosin head. The relevant formulas are derived in the Theory section.

Measuring the combined link stiffness

The principle for measuring the combined series link stiffness, k_L, is to impose a small-amplitude motion on one of the traps and to monitor the resulting motion of both beads, in the absence of myosin. The tension is uniformly distributed in the dumbbell and is measured from the position of the bead in the static trap. The extension of the dumbbell, however, is more prone to error because the link stiffnesses are much greater than the trap stiffnesses, so that the relative motion of the beads is much smaller than the absolute motion of each bead. The extension is therefore critically dependent on the bead position calibrations (V/nm). Using Eq. 10, it can be shown that under typical experimental conditions (trap stiffnesses k_1 and $k_2 = 0.06$ pN/nm, link stiffnesses k_{L1} and $k_{L2} = 1$ pN/nm, myosin stiffness $k_M = 2$ pN/nm), a 10% error in k_L gives a 30% error in k_M.

This source of error was minimized by performing the measurement twice, by oscillating first the right trap and then the left trap, which allows the elimination of the calibrations from the calculation of k_L.

In the case where trap 1 is stationary and trap 2 is driven (Fig. 3 *a*), the condition for the system remaining in equilibrium is expressed most simply by requiring that the change in the tension of the dumbbell equal the change in the force exerted by the stationary trap, i.e., $k_L(\Delta x_2 - \Delta x_1) = k_1 \Delta x_1$ or, equivalently, in terms of the quadrant detector signals and their calibrations ($\Delta x_i \equiv \Delta V_i / cal_i$),

$$m_a \equiv \frac{\Delta V_1}{\Delta V_2} = \frac{\Delta x_1 \times cal_1}{\Delta x_2 \times cal_2} = \frac{cal_1}{cal_2}\left(\frac{k_L}{k_1 + k_L}\right).$$

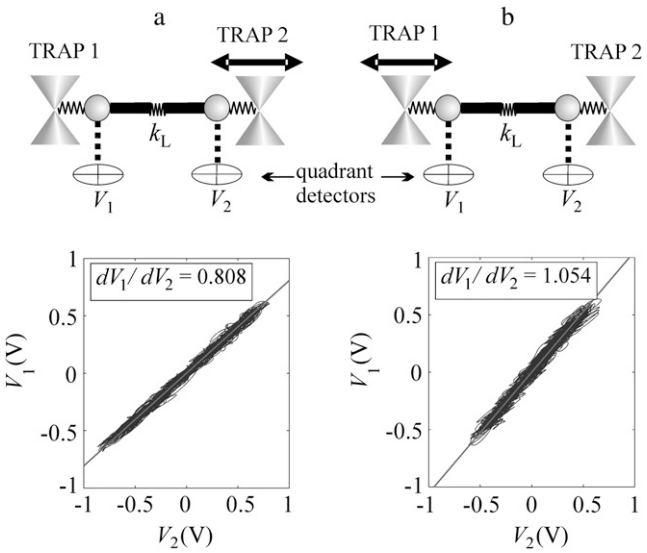

FIGURE 3 Response of the quadrant detector signals upon stretching the dumbbell through (*a*) movement of the trap on the right and (*b*) movement of the trap on the left. The two gradients would symmetrically straddle the value of 1 if the two beads had equal calibration factors and equal trap stiffnesses. Combining the results allows the detector calibrations to be eliminated from the calculation of $k_L = (k_{L1}^{-1} + k_{L2}^{-1})^{-1}$.

The corresponding equilibrium condition for the inverted situation (Fig. 3 *b*), where trap 1 is driven and trap 2 is stationary, is $k_L(\Delta x_2 - \Delta x_1) = -k_2 \Delta x_2$, or

$$m_b \equiv \frac{\Delta V_1}{\Delta V_2} = \frac{\Delta x_1 \times cal_1}{\Delta x_2 \times cal_2} = \frac{cal_1}{cal_2}\left(\frac{k_L + k_2}{k_L}\right).$$

Combining these equations yields k_L independent of the calibrations:

$$k_L = \frac{(k_1 + k_2) + \sqrt{(k_1 + k_2)^2 + 4k_1k_2\left(\frac{m_b}{m_a} - 1\right)}}{2\left(\frac{m_b}{m_a} - 1\right)}$$

$$\frac{cal_1}{cal_2} = \frac{k_1 + k_L}{k_L/m_a}.$$

Theory: the force-extension curve of a single myosin

As the traps are displaced by a distance Δx_T, the tension in the actin filament on either side of the myosin binding site changes by

$$\begin{aligned} \Delta T_1 &= k_1(\Delta x_1 - \Delta x_T) = k_{L1}\Delta x_{L1} \\ \Delta T_2 &= k_2(-\Delta x_2 + \Delta x_T) = k_{L2}\Delta x_{L2}, \end{aligned} \quad (3)$$

respectively, relative to the tension and the trap and bead positions at the time of attachment. The total force experienced by the myosin head resulting from the movement of the traps is then given by

$$F_M = \Delta T_1 - \Delta T_2. \quad (4)$$

The extension of the myosin head requires the extension of each actin-bead link, and these are not directly measurable:

$$x_M = \Delta x_1 + \Delta x_{L1} = \Delta x_2 - \Delta x_{L2}. \quad (5)$$

Equations 2 and 3 give

$$\Delta x_{L2} = \frac{\Delta T_2}{k_L k_{L1}}(k_{L1} - k_L), \quad (6)$$

and with Eq. 5 we obtain

$$\Delta x_{L1} = \Delta x_2 - \Delta x_1 - \frac{\Delta T_2}{k_L k_{L1}}(k_{L1} - k_L). \quad (7)$$

Using $\Delta T_1 = k_{L1}\Delta x_{L1}$ to eliminate k_{L1} gives

$$\Delta x_{L1} = \frac{\Delta T_1}{\Delta T_1 - \Delta T_2}\left(\Delta x_2 - \Delta x_1 - \frac{\Delta T_2}{k_L}\right), \quad (8)$$

which yields

$$x_M = \frac{\Delta T_1 \Delta T_2}{\Delta T_1 - \Delta T_2}\left(\frac{\Delta x_2}{\Delta T_2} - \frac{\Delta x_1}{\Delta T_1} - \frac{1}{k_L}\right). \quad (9)$$

The force-extension curve is obtained by plotting F_M versus x_M as shown in Fig. 4 *b*. In practice, the most convenient method for deducing k_M is to use the parameters R_1 and R_2 (Eq. 1), where, in effect, Brownian noise is averaged out at the first step of analysis. Thus,

$$\begin{aligned} \Delta x_1 &= R_1 \Delta x_T \\ \Delta x_2 &= R_2 \Delta x_T \\ \Delta T_1 &= -k_1(1 - R_1)\Delta x_T \\ \Delta T_2 &= +k_2(1 - R_2)\Delta x_T. \end{aligned}$$

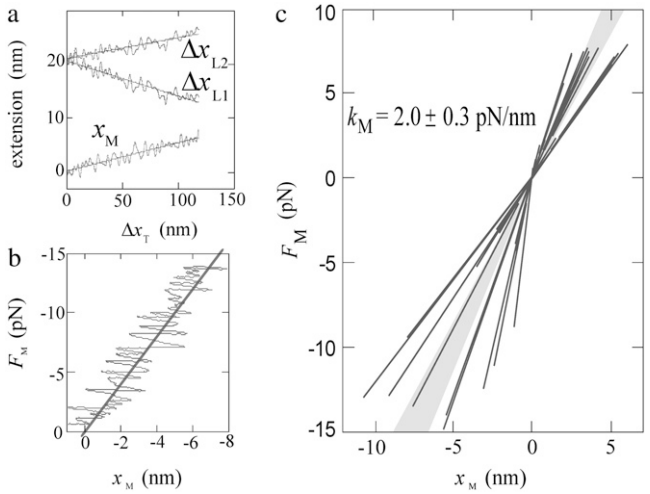

FIGURE 4 Force-extension curve for a single myosin head. (*a*) Extension of the elastic elements (links and myosin) in response to the applied trap motion Δx_T during a single bound period. For this dumbbell, $k_{L1} = 0.90$ pN/nm and $k_{L2} = 1.70$ pN/nm. (*b*) The myosin force-extension curve for this bound period, corresponding to $k_M = dF_M/dx_M = 2.2$ pN/nm. The fit was obtained from the regression of x_M on F_M because the dominant noise was on the x_M axis. (*c*) The linear fits for the bound periods in the 100-s data record. The shaded region indicates the error in the mean stiffness, $k_M = 2.0 \pm 0.3$ pN/nm, obtained from the ensemble of events for this record using Eq. 10.

Substituting these expressions into Eqs. 4 and 9 gives

$$k_M = \frac{F_M}{x_M} = \frac{[k_1(1-R_1)+k_2(1-R_2)]^2}{k_1R_2(1-R_1)+k_2R_1(1-R_2)-\frac{k_1k_2}{k_L}(1-R_1)(1-R_2)}. \quad (10)$$

The covariance method

The details of this method have already been published (9), but, as described in the Appendix, a correction is needed if data are collected over too narrow a bandwidth. For our conditions ($k_1 = k_2 = 0.06$ pN/nm, $k_{L1} = k_{L2} = 1$ pN/nm, and assuming $k_M = 2$ pN/nm), the bandwidth of the covariance is 4.2 kHz, which for a collection bandwidth of 5 kHz only yields 80% of the total bound-state covariance. This necessitates a reduction in the estimate of k_M by 30%. If we assume instead that the myosin is less stiff (e.g., 0.3 pN/nm for a slow myosin (10)) the bandwidth of the covariance is 1.7 kHz and the corresponding correction is down to 10%. Data collection at higher frequency would have avoided the need for correction but as the process is simple, it is not worth storing the significantly bigger files. This optimal measurement bandwidth covers essentially all the spectrum corresponding to the unbound state (corner frequency ~2 kHz) while somewhat reducing the fraction of the spectrum arising from bound state (>10 kHz).

Protocol

Methods of rabbit actin and myosin S1 preparation have already been described, as has the optical trap setup (20). For these experiments S1 was attached directly to nitrocellulose. The methods of actin biotinylation and neutravidin attachment to carboxy beads were also reported in that publication. Electrooptic deflectors of 2-mm aperture (Leysop, Essex, UK) were used to change the trap positions, which were computer-controlled via Labview (National Instruments, Austin, TX). Trap stiffnesses of ~0.06 pN/nm were used and, for most experiments, 2 μM ATP.

The validity of the ramp method was tested in the following manner. First, the dumbbell was tensioned sufficiently to allow detection of binding events. The quadrant detectors were calibrated (21) and the direction of the working stroke (and hence the polarity of actin) was determined by detecting events while the dumbbell was moved slowly past the myosin over a distance covering five actin target zones (5 × 37 nm). This record also yielded the estimate of the myosin and link stiffnesses based on the covariance method. The combined link stiffness was measured and the ramp method was then used to characterize the myosin force-extension curve. At this point the dumbbell was stretched further by increasing the trap separation so as to increase the tension, and, consequently, the stiffness of the actin-bead links. The procedure was then repeated so as to get measurements of myosin and bead-link stiffnesses independently by the two methods at each dumbbell tension.

RESULTS

The myosin force-extension curve and stiffness, k_M, using the ramp method

Three parameters, the combined link stiffnesses and the two values R_1 and R_2, are required to deduce (using Eqs. 3–9) the extension of the myosin spring and of the actin-bead links as a function of force. Fig. 4 *a* is an example of a particularly long-lived bound state and shows the linearity of the elements over a wide extension range, consistent with the assumptions of the model. Because the trap stiffnesses k_1 and k_2 are an order of magnitude smaller than the other elastic elements in the system, the actin-bead links and the myosin are only stretched to a small extent relative to the displacement of the traps, and this is reflected in the difference between the scales on the horizontal and vertical axes. The gradient of Δx_{L1} is greater than that of Δx_{L2}, because for this dumbbell k_{L1} (0.90 pN/nm) < k_{L2} (1.70 pN/nm). The three gradients in Fig. 4 *a* are similar in magnitude, which shows the necessity of accurate measurement of all the compliant elements. The force-extension curve for the myosin head corresponding to this event is shown in Fig. 4 *b*, and demonstrates Hookean behavior over a range of 0–14 pN (~7 nm), with a gradient of $k_M = 2.2$ pN/nm for this particular bound state.

As explained previously, the most convenient way of computing k_M is to fit the raw data to straight lines to obtain R_1 and R_2, the factors by which the bead motions are slowed during interactions with the stiff myosin (see Fig. 2 and Eq. 1). Their mean values were then substituted into Eq. 10, along with their standard error, to yield k_M. The average value of k_M deduced in this manner from a single 100-s record is 2.0 ± 0.3 pN/nm (56 binding events), and is represented as the shaded region in Fig. 4 *c*. The straight lines distributed around this region in the figure represent the fits for the individual bound states. There was no significant difference in the average k_M values corresponding to forces assisting ($F_M < 0$) or resisting ($F_M > 0$) the working stroke. The average k_M values obtained for all the records are displayed in Fig. 5.

The value of k_M should be independent of the value of k_L (adjusted by tensioning the dumbbell) and this test is shown in Fig. 5. The estimate of myosin stiffness is reasonably independent of the value of the combined link stiffness.

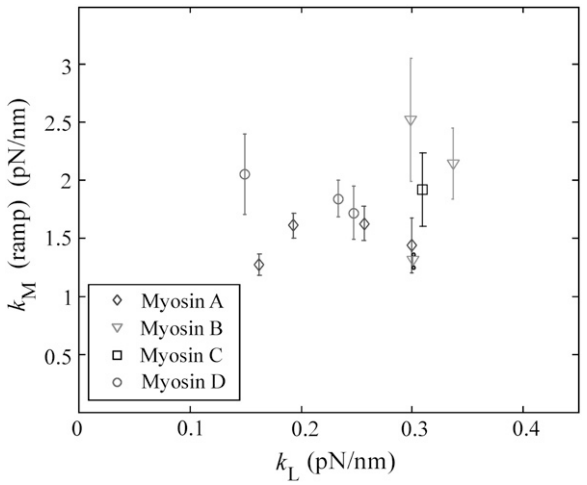

FIGURE 5 Effect of tensioning the dumbbell on the estimate of k_M. The nonlinear nature of the actin-bead links means that tensioning the dumbbell increases the combined link stiffness, k_L, but the myosin stiffness should of course remain constant. The data come from four different myosin molecules and the error bars result from the spread of values of R_1 and R_2 substituted into Eq. 10.

Comparison of the ramp and covariance methods

The values of k_M estimated from the ramp method are compared with the estimates from the covariance method in Fig. 6, the pair of data traces being taken in quick succession.

The average value from all the measurements using the ramp method was 1.7 ± 0.3 pN/nm (four myosins, 1080 interactions), a result obtained from the weighted average of the values in Fig. 5 (weight = 1/error^2). The mean k_M for the covariance method was 2.1 ± 0.1 pN/nm (the same four myosins, eleven 100-s records, ~2500 interactions), so although there was fair agreement between the two methods, the covariance method gave slightly higher estimates.

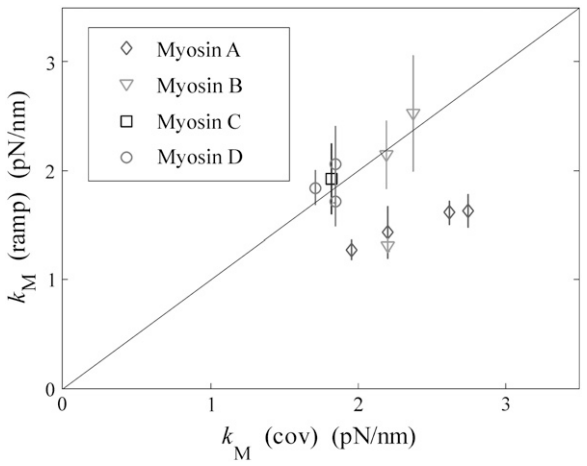

FIGURE 6 Comparison of the estimates of k_M from the ramp and covariance methods. The two methods were applied in quick succession to each dumbbell-myosin pair for each dumbbell tension. The points lie fairly close to the line of unit gradient.

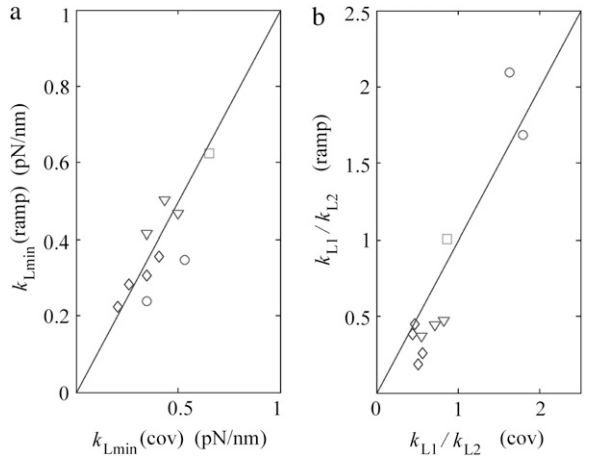

FIGURE 7 Comparison of link stiffness measurements by the ramp and covariance methods. (*a*) Estimate of the stiffness of the weaker of the two links using the ramp method plotted against the estimate using the covariance method. (*b*) Ratio of link stiffnesses from the ramp method versus ratio from the covariance method.

Estimates of the values of link stiffness by the ramp and the covariance methods are compared in Fig. 7 and the agreement can be seen to be fairly satisfactory, since the points are distributed close to the line of unit gradient. Fig. 7 *a* shows the stiffness of the weaker of the two links and Fig. 7 *b* the ratio of link stiffnesses. The two links of the dumbbell are generally not equal.

Estimate of k_M from a larger number of myosin molecules using the covariance method

Having established that the estimates for k_M from the two methods were fairly similar we went back over some old records to extract k_M for more myosin molecules using the covariance method with bandwidth correction. Data traces for which the bound periods were poorly identified (i.e., where the contrast between bound and unbound variances was small) were discarded to avoid including myosins that were weakly bound to the substrate. The resulting distribution is shown in Fig. 8. For a set of 166 different myosin molecules, the mean value of k_M was 1.79 pN/nm, with SD = 0.7 pN/nm and a corresponding SE = 0.06 pN/nm. The distribution is slightly skewed and it seemed possible that the high values, which are almost double the mean, could arise from the attachment of more than one head. However, if two heads did attach, the two ATP-binding and actin-dissociation events would very likely be independent, in which case the final time interval of an event would be expected to be associated with a higher variance than with the earlier, two-headed part. We found no sign of this effect when examining several records, for which the estimate of k_M was particularly high, and we conclude that two-headed binding is not the source of the skewed distribution.

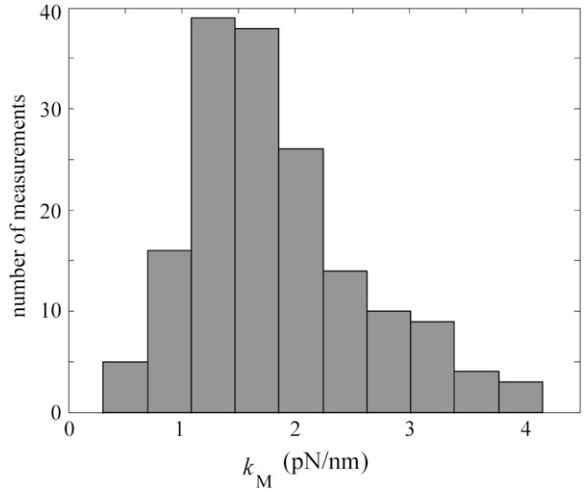

FIGURE 8 Histogram of values of k_M obtained from 166 different myosin molecules using the covariance method. Mean = 1.79 pN/nm, SD = 0.7 pN/nm; SE = 0.06 pN/nm.

Strain-dependent lifetime of bound periods

The ramp method also reveals a strain dependence of the detachment rate. Fig. 9 *a* is a record of bead position during one cycle of the imposed triangle wave. The beads are pulled out of the traps in either the positive or negative direction, depending on the phase of the wave, and the force F_M on the myosin head during each bound period (see Fig. 9 *b*) is given by Eq. 4. A positive force corresponds to resistance to the working stroke. When F_M is plotted for the entire 100-s duration of a data record (inset of Fig. 9 *c*), an asymmetry in the lifetimes of the bound periods is revealed with respect to the sign of the applied force. The maximum force excursions are smaller on the side corresponding to resisting (positive) forces, indicating a faster rate of release. This asymmetry is summarized in the histogram of peak forces shown in Fig. 9 *c*, taken from nine 100-s data records for one typical myosin molecule.

In an experiment with static traps, the bound periods are terminated by the binding of ATP, and the default interpretation for the asymmetry in Fig. 9 *c* is a strain-dependent rate of ATP binding, $k_{detach}(F) = k^0_{detach}\exp(Fd/k_BT)$. The solid curve overlaid on the histogram is obtained by integrating this rate over the time course of the imposed force, and yields $d \approx 1$ nm. However, it is likely that this ATP-mediated detachment is not the only pathway of dissociation, as Fig. 9 *d* shows three occurrences of immediate rebinding. Such events almost certainly correspond to a ripping off of a rigor cross-bridge followed by a rapid rebinding of the apomyosin. It is known from solution studies that the apomyosin binds orders of magnitude more rapidly than the M.ADP.Pi state, which would rebind in the standard cross-bridge cycle.

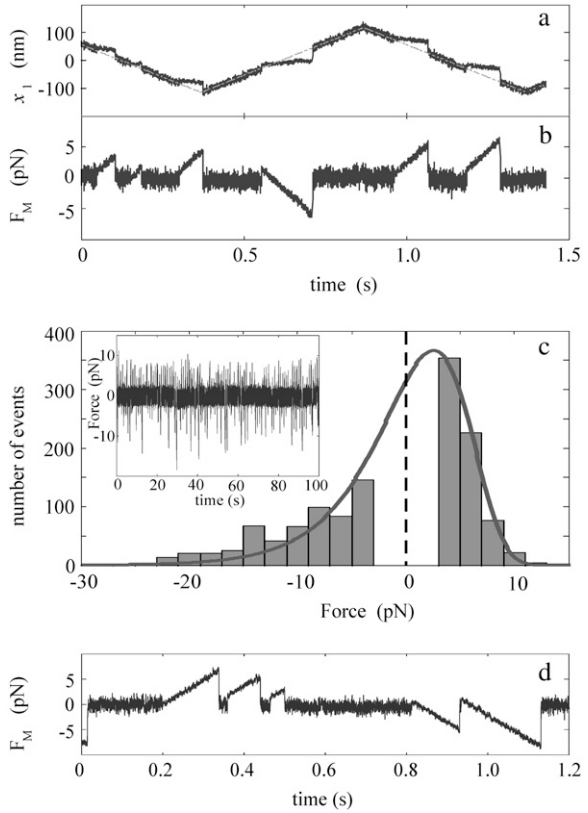

FIGURE 9 Asymmetry in the duration of interactions. (*a*) Bead positions during interactions. (*b*) Resultant forces during the same interactions. (*c*) Histogram of peak forces observed for nine 100-s records on a single myosin, showing a clear asymmetry between the magnitudes of the positive forces and the negative forces. The gap in the histogram around zero force arises because only events with peak forces significantly outside the thermal noise were included. The solid curve is the theoretical fit for the simplest strain-dependent kinetics and corresponds to an interaction distance of ~1 nm, but is included primarily to lead the eye through the data. (*Inset*) A 100-s force record directly displaying the asymmetry between the positive and negative forces. (*d*) A record showing immediate rebinding after dissociation of actin, consistent with ripping off of rigor cross-bridges followed by rapid rebinding of apomyosin.

DISCUSSION

For single-molecule studies to play a more significant part in understanding the cross-bridge cycle of skeletal myosin, it would help if the estimates of the basic parameters, the size of the working stroke and the stiffness of the myosin cross-bridge, were in reasonable agreement with those from fiber studies. In single-molecule studies, the myosin is held in an artificial manner and the onus is on this method to justify its values, since the estimates of both the working stroke and the myosin stiffness, obtained from fiber experiments, can be strongly defended. The estimate of the myosin stiffness comes from the measurements of fiber stiffness, which are largely unchanged since the reports of Huxley and Simmons in 1971 (1). The aspect that has changed is the contribution of actin and myosin filament compliance to the overall fiber compliance, but there is substantial agreement between several groups on this issue. For the most experimentally favorable muscle, that of frog, the best estimate is 3.3 pN/nm, and it would be difficult to support a value of <2 pN/nm. It is

interesting that the estimate for rabbit fibers is 1.7 pN/nm (12), which is significantly less than for frog fibers.

The relation of the stiffness of the cross-bridge, k_M, to the size of the working stroke, h, is crucial for modeling of cross-bridge action, because the work, $\frac{1}{2}(k_M h^2)$, in general appears in an exponent, and a doubling of stiffness has a dramatic effect on the working of any realistic model.

When considering muscle fiber data, a more useful expression for the energy is $\frac{1}{2}(F^2/k_M)$ (F being the applied force), because there is no uncertainty about the isometric force of a muscle fiber, and there is increasing agreement that the fraction of heads bound is in the range 30–40%. The resulting estimate is 5 pN/head. The free energy of ATP hydrolysis is 80 pN nm, and the efficiency of frog muscle under optimal conditions is ~45% (22), so if the working stroke were to take place in a single step, one would expect a stiffness of $\sim\frac{1}{2}(5\text{ pN})^2/(80\text{ pN nm} \times 0.45) = 0.35$ pN/nm, considerably lower than our observed value of 1.7 pN/nm and in even worse agreement with the stiffness of myosin heads in frog fibers. This argument has been fully presented by Decostre et al. (7), with the conclusion that the working stroke must consist of a number of substeps (or, alternatively, take place in a concerted fashion) and is outlined here merely to emphasize the significance of cross-bridge stiffness for muscle models.

As was first shown by Dupuis et al. (18), the widely used dumbbell method for investigating individual interactions of a myosin head and an actin monomer suffers from series compliant elements. For muscle fibers, the problem is caused by the actin and myosin filaments, whereas for the dumbbell experiments it is the actin-bead links. The force-extension curve of the actin-bead links is nonlinear, so that pre-tensions of 5–10 pN are required for easy detection of myosin-binding events based on the reduction of the variance of bead position. Knowledge of the stiffness of the actin-bead links is essential for measuring the stiffness of the myosin head and is also required for correcting the estimate of the working stroke. Smith et al. described the covariance method for determining the three values of stiffness based on measurement of the autovariance and covariance of the bead positions during bound and free periods. This method requires no extra measurements beyond those routinely taken in a record of actomyosin interactions. Despite its simplicity, the method has not been widely used and the values of link stiffness are rarely reported. One of the functions of this article was to help validate this convenient method by comparing it in detail with the new ramp method. A useful outcome of this comparison is that we now appreciate the relatively high sampling frequency required to accurately measure the covariance during bound periods and also the most likely source of error, correlated noise between the beads.

The ramp method gives an average myosin head stiffness of 1.7 ± 0.3 pN/nm, in fair agreement with the result of the covariance method, 2.1 ± 0.1 pN/nm, measured from the same four molecules. Extending the covariance result to many more molecules yields 1.79 ± 0.06 pN/nm. These values are satisfyingly consistent with the most recent estimates from rabbit fiber experiments (1.7 pN/nm) (12), but there are two aspects of the dumbbell experiment that differ from the circumstances in vivo. First, the value of k_M would be an underestimate if the attachment of the myosin to the nitrocellulose surface provided an additional source of compliance. Second, any compliance from parts of the myosin molecule other than S1 is eliminated, leading to the possibility of an overestimate of cross-bridge stiffness. Although it has been suggested in the past that melting of the α-helices of the S2 part of myosin might contribute to both the working stroke and the compliance of the myosin head (23), the observation that Sl is fully competent for the actin motility assay (24) made this considerably less plausible.

There have been a number of earlier single-molecule measurements of the compliance of myosin. Nishizaka et al. (13) reported a value for k_M of 0.6 pN/nm but the direction of the pulling force was not as well defined as in the current work. Mehta et al. (14) used the change of correlation of the two trapped beads and reported an estimate of 0.65 pN/nm. Veigel et al. (8) applied a small-amplitude sine wave to one of the beads and compared the transmission of the wave to the second bead when the myosin head was either bound or free, and they reported a value of 0.7 pN/nm. They assumed that both bead link stiffnesses were the same, which may contribute to their lower estimate of k_M, since in general, for our biotin-neutravidin links, we do not find this to be the case (see Fig. 7 *b*). Our link stiffnesses were higher than those of other investigators, which facilitates the characterization of a stiff myosin. We note that both Mehta and Veigel used HMM rather than Sl and this could contribute to their lower estimates of myosin stiffness. There have been a couple of more recent studies in which stiffer biotin-avidin actin-bead links were used, and from modeling of the overall response, significantly higher values of myosin stiffness were deduced (i.e., 1.3 pN/nm (11) and 1.1 pN/nm (10)).

The covariance method is attractive in that values of stiffness can be more directly related to the measured co- and autovariances. If, as should be the case, the values of trap stiffness are significantly less than those for myosin and the links, a useful approximation for the myosin stiffness is $k_M \approx (k_1+k_2)\times cov_{\text{unbound}}/cov_{\text{bound}}$. During free periods, the dumbbell can be approximated to a rigid rod and, as expected, the covariance is roughly equal to the autovariances of the two beads. The covariance during the bound periods is relatively small but is immune to uncorrelated (e.g., shot) noise. The potentially serious source of error is correlated noise, which would serve to reduce the estimate of myosin stiffness. Two obvious sources are arc lamp flicker and stage noise. The importance of the first source was checked by measuring the covariance with a slack dumbbell and was found to be negligible (although the performance of the xenon arc does need to be checked from time to time). Stage noise occurs predominantly at low frequency and was filtered out as described in Methods. Each bead-link stiffness is

primarily governed by the autovariance of that bead during bound periods.

For the ramp method, the values of stiffness can be somewhat less clearly associated with the three parameters, the combined link stiffnesses, k_L, and R_1 and R_2. The weaker of the two links is primarily governed by k_L, and the value of myosin stiffness is primarily governed by the smaller of the two values of R. For dumbbells in which the values of link stiffness are very different, the errors in the estimate of the strong link become significant.

The ramp method has the merit of exploring the force-extension curve over the full physiological range. The linearity of the bead motions during bound periods (Figs. 2 and 9 *b*) is a notable feature of our data and is consistent with all the elastic elements in the system being Hookean over the range of strains explored. In apparent contradiction with this inference, there have been reports of significant nonlinearity in the actin-bead links (9,18). The force-extension curve in Fig. 8 of Smith et al. can be reasonably fitted with an exponential dependence, the link stiffness doubling with about every 9 nm of extension. However, detailed analysis of our data collected to measure the combined link stiffness (Fig. 3) provides no evidence for curvature over the limited range of forces (~3 pN), indicating that the nonlinearity of the links used in the experiments described here was significantly less than that of experiments described earlier. Simulation of the ramp experiment showed that links with nonlinearity of the strength reported by Smith et al. would result in a clearly measurable nonlinear motion of the beads during bound periods, which we do not observe. This supports our inference that the links were not as nonlinear as those reported earlier. Introducing a weak nonlinear behavior in the traps (k_1 and k_2 decreasing with increasing strain (19)) would further aggravate the nonlinearity in both bead signals. The additional effect of nonlinear motion in the myosin head has opposite effects on the bead bearing increasing and that bearing decreasing tension. The nonlinear motion for the former bead is aggravated, whereas that for the latter bead is attenuated. We conclude that the observed linearity in the bead signals cannot result from a fortuitous cancellation of effects arising from nonlinearity in the individual elements. The data presented here is consistent with the springs being near-Hookean in character, but to quantitate the extent of nonlinearity would require some careful, dedicated experiments that are beyond the scope of this study.

The forces observed during the ramp experiments also directly show an asymmetry that must result from a dependence of the dissociation kinetics upon strain. The method is straightforward to apply in that it does not require rapid event detection and imposition of defined forces on the actomyosin bond (25) but histograms of the type shown in Fig. 9 *c* would have been needed for a range of ATP concentrations to characterize the likely involvement of two pathways. Nishizaka et al. (13) investigated the effect of strain on breaking the actomyosin bond under strictly rigor conditions. In their experiment, the direction of the applied force was not strictly along the axis of the working stroke, and they were unable to distinguish the effects of positive and negative forces. Nonetheless, their rate of rigor bond breaking would lend significant support to our observed rates. We note that Veigel et al. (25), working on smooth-muscle myosin, reported that the application of forces assisting the working stroke accelerated the rate of dissociation, which is the opposite of the effect we observe with skeletal myosin. This could result from dependence of the dominant pathway of dissociation on the type of myosin and on experimental conditions.

APPENDIX: MEASURING THE MYOSIN STIFFNESS FROM THE BEAD POSITION COVARIANCE

The method for measuring stiffnesses from the variance and covariance of the beads in the bound and unbound states provides an alternative measurement of the myosin stiffness, k_M, and the link stiffnesses, k_{L1} and k_{L2}, with which to compare the results of the ramp method. The theory (9) assumes that the bead positions are measured over their full bandwidth. In fact, the value of k_M is sufficiently large that the power spectrum of the beads during bound periods spreads significantly further than the bandwidth (5 kHz) that is routinely used for these experiments and that is convenient for optimizing event detection. (For the unbound case, the power spectrum lies comfortably within the measurement bandwidth with a corner frequency of ~2 kHz.) This results in an underestimate of the covariance for bound periods and, consequently, an overestimate of k_M. To improve the accuracy of the k_M, k_{L1}, and k_{L2} measurements, the ''covariance'' method was amended to compensate for this effect.

On the basis of the linear-springs model in Fig. 1 (9),

$$\mathrm{var}(x_1)_{\mathrm{bound}} = \frac{k_M + k_{L1} + \tilde{k}_{L2}}{(k_1 + k_{L1})(k_M + \tilde{k}_{L1} + \tilde{k}_{L2})} k_B T$$

$$\mathrm{var}(x_2)_{\mathrm{bound}} = \frac{k_M + k_{L2} + \tilde{k}_{L1}}{(k_2 + k_{L2})(k_M + \tilde{k}_{L1} + \tilde{k}_{L2})} k_B T$$

$$\mathrm{cov}(x_1, x_2)_{\mathrm{bound}} = \frac{k_{L1} k_{L2}}{(k_1 + k_{L1})(k_2 + k_{L2})(k_M + \tilde{k}_{L1} + \tilde{k}_{L2})} k_B T,$$

where $\tilde{k}_{L1} = k_1 k_{L1}/k_1 + k_{L1}$ and a similar expression holds for $\tilde{k}_{L2}$. (The above equations were amended to cater to unequal trap stiffnesses k_1 and k_2.) The corresponding expressions for the case of unbound dumbbells are obtained by substituting $k_M = 0$ in the above equations. A numerical solution for k_M can then be computed from the variance ratios

$$A_{11} = \frac{\mathrm{var}(x_1)_{\mathrm{unbound}}}{\mathrm{var}(x_1)_{\mathrm{bound}}}, \quad A_{22} = \frac{\mathrm{var}(x_2)_{\mathrm{unbound}}}{\mathrm{var}(x_2)_{\mathrm{bound}}}, \quad \text{and}$$

$$A_{12} = \frac{\mathrm{cov}(x_1, x_2)_{\mathrm{unbound}}}{\mathrm{cov}(x_1, x_2)_{\mathrm{bound}}}. \tag{11}$$

The random thermal forces $F_1(t)$ and $F_2(t)$ acting on the beads can be written as

$$F_1 = k_1 x_1 - k_{L1} x_{L1} + \beta \frac{dx_1}{dt}$$

$$F_2 = k_2 x_2 + k_{L2} x_{L2} + \beta \frac{dx_2}{dt},$$

where β is the hydrodynamic drag coefficient, or in frequency space as

$$\hat{F}_1 = k_1\hat{x}_1 + 2\pi i f\beta\hat{x}_1 - k_{L1}(\hat{x}_M - \hat{x}_1)$$
$$\hat{F}_2 = k_2\hat{x}_2 + 2\pi i f\beta\hat{x}_2 - k_{L2}(\hat{x}_2 - \hat{x}_M), \qquad (12)$$

where $\hat{x}_1(f) = \int_{-\infty}^{\infty} x_1(t)e^{2\pi i f t}dt$, with similar expressions for $\hat{x}_2(f)$, $\hat{x}_M(f)$, $\hat{F}_1(f)$, and $\hat{F}_2(f)$. The length of the filament on either side of the myosin binding point, x_M, is irrelevant for this calculation, so that the lengths of the actin-bead links can be expressed as $x_{L1} = x_M - x_1$ and $x_{L2} = x_2 - x_M$ without loss of generality.

Equation 12 can then be rewritten as

$$\begin{pmatrix}\hat{F}_1\\ \hat{F}_2\end{pmatrix} = \begin{pmatrix}a + 2\pi i f\beta & -b\\ -b & c + 2\pi i f\beta\end{pmatrix}\begin{pmatrix}\hat{x}_1\\ \hat{x}_2\end{pmatrix}$$

or, equivalently, as

$$\begin{pmatrix}\hat{x}_1\\ \hat{x}_2\end{pmatrix} = \frac{1}{\Delta(f)}\begin{pmatrix}c + 2\pi i f\beta & b\\ b & a + 2\pi i f\beta\end{pmatrix}\begin{pmatrix}\hat{F}_1\\ \hat{F}_2\end{pmatrix},$$

where

$$a = k_1 - \frac{k_{L1}^2}{\Sigma} + k_{L1};$$
$$b = \frac{k_{L1}k_{L2}}{\Sigma};$$
$$c = k_2 - \frac{k_{L2}^2}{\Sigma} + k_{L2};$$
$$\Sigma = k_{L1} + k_{L2} + k_M; \quad \text{and}$$
$$\Delta(f) = (a + 2\pi i f\beta)(c + 2\pi i f\beta) - b^2.$$

The power spectra P_{11} and P_{22} and the cross-spectrum P_{12} for the bead positions are given by

$$P_{11}(f) = |\hat{x}_1(f)|^2 = \frac{|c + 2\pi i f\beta|^2|\hat{F}_1|^2 + b^2|\hat{F}_2|^2}{|\Delta(f)|^2};$$
$$P_{22}(f) = |\hat{x}_2(f)|^2 = \frac{|a + 2\pi i f\beta|^2|\hat{F}_2|^2 + b^2|\hat{F}_1|^2}{|\Delta(f)|^2};$$
$$\hat{x}_1(f)\hat{x}_2^*(f) = \frac{b(c + 2\pi i f\beta)|\hat{F}_1|^2 + b(a - 2\pi i f\beta)|\hat{F}_2|^2}{|\Delta(f)|^2}; \quad \text{and}$$
$$P_{12}(f) = \mathrm{Re}\left[\hat{x}_1(f)\hat{x}_2^*(f)\right] = \frac{b(c|\hat{F}_1|^2 + a|\hat{F}_2|^2)}{|\Delta(f)|^2}, \qquad (13)$$

where the asterisk denotes the complex conjugate. Only the real part of $\hat{x}_1(f)\hat{x}_2^*(f)$ contributes to the covariance, because the imaginary parts cancel out when, in performing the inverse Fourier transform, the integration covers both negative and positive f. Because the beads are identical, and F_1 and F_2 have constant white-noise power spectra, $|\hat{F}_1|^2 = |\hat{F}_2|^2$. The above equations yield two sets of power spectra corresponding to the filament being bound or unbound to myosin. The latter case is obtained by substituting $k_M = 0$.

The total variances and covariance are then obtained by integrating P_{11}, P_{22}, and P_{12}. Use of a restricted bandwidth Ω results in an underestimate of the true values.

Fig. 10 *a* shows the expected deviations of the computed values of k_M and $k_L = (k_{L1}^{-1} + k_{L2}^{-1})^{-1}$ from their true values, resulting from the finite bandwidth in the absence of any correction, for set values of $k_1 = k_2 = 0.06$ pN/nm, $k_{L1} = k_{L2} = 1$ pN/nm ($k_L = 0.5$ pN/nm), and $k_M = 2$ pN/nm. These results were obtained by calculating the values of the variance ratios expected from the finite bandwidth Ω.

$$A_{ij}(\Omega) = \frac{\int_0^\Omega P_{ij}[\text{unbound}]df}{\int_0^\Omega P_{ij}[\text{bound}]df} \quad i,j = 1,2. \qquad (14)$$

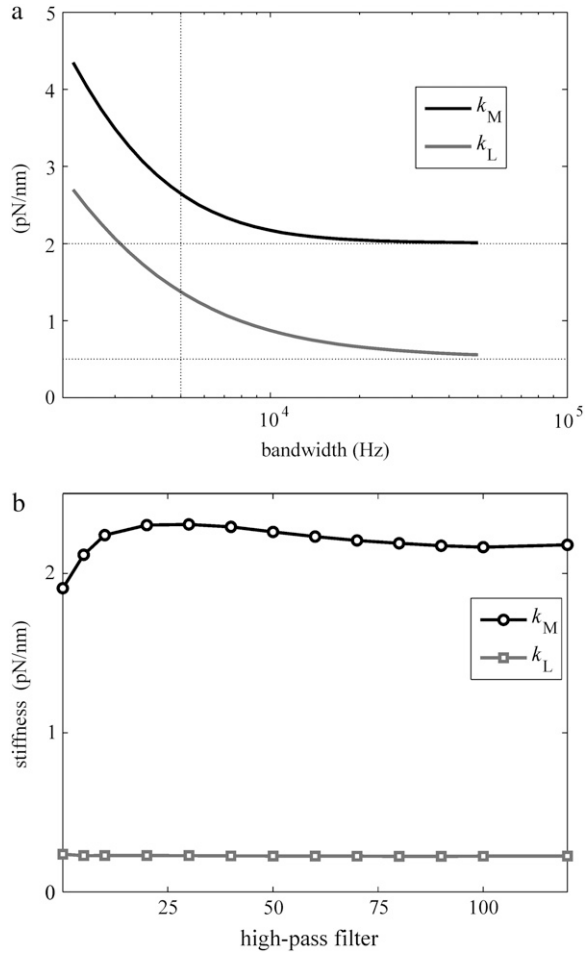

FIGURE 10 Effects of sampling bandwidth on the calculation of k_M and k_L using the covariance method. (*a*) Theoretical deviations of k_M and k_L from their true values (the asymptotic value at infinity) as a result of finite measurement bandwidth. $k_1 = k_2 = 0.06$ pN/nm, $k_{L1} = k_{L2} = 1$ pN/nm ($k_L = 0.5$ pN/nm), and $k_M = 2$ pN/nm. The vertical dotted line shows the 5-kHz limit of this experiment. (*b*) Example of the effect of filtering out spurious low-frequency non-Brownian noise from the raw data, on the measurement of k_M and k_L. Two tendencies are discernible: a positive correction, resulting from correlated noise (possibly due to instability of stage or xenon arc) and a negative one, resulting from anticorrelated noise (from an unknown source).

Integrating the power spectra in this manner corresponds to applying a ''top-hat'' filter to the experimental data, with a cut-off frequency Ω, a suitable approximation to the eight-pole anti-aliasing filters used in our measurements. The uncorrected values are significantly overestimated at the measurement bandwidth, 5 kHz, used in the experiments described here.

We have corrected for this factor by using an iterative algorithm. Starting from a first estimate of k_M, k_{L1}, and k_{L2}, power spectra were calculated from Eq. 13 and integrated up to 5 kHz. From the resulting values of A_{ij}, the stiffness estimates were modified and this procedure was repeated until self-consistency was achieved between k_M, k_{L1}, k_{L2}, A_{ij}, and Ω. As a test for the validity of this method, it was applied to a set of experimental data that was measured with a large bandwidth (25 kHz) and filtered numerically. The correction procedure significantly reduced the error in k_M from 80% to 20%.

Contributions to systematic error from the low-frequency range were also considered. For long events, low-frequency noise of a magnitude significantly larger than that expected from Brownian noise is sometimes evident. Some of this noise is correlated between the two beads, possible sources being instability in the xenon arc or mechanical vibrations in the microscope

stage. Such noise produces an increase in the measured bound covariance that results in an underestimate of the real myosin stiffness. This noise is limited to a band of frequencies that is much narrower than the overall bandwidth of the spectra (Eq. 13), and can therefore be filtered out without significantly affecting the total variance (Eq. 14). Fig. 10 *b* shows, for one sample of data, the variation in the measurement of k_M and k_L obtained for a range of filter cut-offs. After an initial increase, k_M subsequently decreases before reaching a plateau. The decrease in k_M indicates an anticorrelated component in the non-Brownian noise, but the source of this is unkown. The correction to k_M varied from 0 to 10% depending on the sample. Filtering was generally found to affect the k_L measurement negligibly. It should be noted that in the programs made available by Smith et al. (9), the covariances were calculated for each window, which effectively filters out this low-frequency component.

This work was funded by the Medical Research Council.

REFERENCES

1. Huxley, A. F., and R. M. Simmons. 1971. Proposed mechanism of force generation in striated muscle. *Nature*. 233:533–538.
2. Kojima, H., A. Ishijima, and T. Yanagida. 1994. Direct measurement of stiffness of single actin filaments with and without tropomyosin by in vitro nanomanipulation. *Proc. Natl. Acad. Sci. USA*. 91:12962–12966.
3. Huxley, H. E., A. Stewart, H. Sosa, and T. Irving. 1994. X-ray diffraction measurements of the extensibility of actin and myosin filaments in contracting muscle. *Biophys. J*. 67:2411–2421.
4. Wakabayashi, K., Y. Sugimoto, H. Tanaka, Y. Ueno, Y. Takezawa, and Y. Amemiya. 1994. X-ray diffraction evidence for the extensibility of actin and myosin filaments during muscle contraction. *Biophys. J*. 67:2422–2435.
5. Huxley, A. F., V. Lombardi, and L. D. Peachey. 1981. A system for fast recording of longitudinal displacement of a striated muscle fiber. *J. Physiol*. 317:P12–P13.
6. Reconditi, M., M. Linari, L. Lucii, A. Stewart, Y. B. Sun, P. Boesecke, T. Narayanan, R. F. Fischetti, T. Irving, G. Piazzesi, M. Irving, and V. Lombardi. 2004. The myosin motor in muscle generates a smaller and slower working stroke at higher load. *Nature*. 428:578–581.
7. Decostre, V., P. Bianco, V. Lombardi, and G. Piazzesi. 2005. Effect of temperature on the working stroke of muscle myosin. *Proc. Natl. Acad. Sci. USA*. 102:13927–13932.
8. Veigel, C., M. L. Bartoo, D. C. White, J. C. Sparrow, and J. E. Molloy. 1998. The stiffness of rabbit skeletal actomyosin cross-bridges determined with an optical tweezers transducer. *Biophys. J*. 75:1424–1438.
9. Smith, D. A., W. Steffen, R. M. Simmons, and J. Sleep. 2001. Hidden-Markov methods for the analysis of single-molecule actomyosin displacement data: the variance-Hidden-Markov method. *Biophys. J*. 81: 2795–2816.
10. Capitanio, M., M. Canepari, P. Cacciafesta, V. Lombardi, R. Cicchi, M. Maffei, F. S. Pavone, and R. Bottinelli. 2006. Two independent mechanical events in the interaction cycle of skeletal muscle myosin with actin. *Proc. Natl. Acad. Sci. USA*. 103:87–92.
11. Takagi, Y., E. E. Homsher, Y. E. Goldman, and H. Shuman. 2006. Force generation in single conventional actomyosin complexes under high dynamic load. *Biophys. J*. 90:1295–1307.
12. Linari, M., M. Caremani, C. Piperio, P. Brandt, and V. Lombardi. 2007. Stiffness and fraction of myosin motors responsible for active force in permeabilized muscle fibers from rabbit psoas. *Biophys. J*. 92:2476–2490.
13. Nishizaka, T., H. Miyata, H. Yoshikawa, S. Ishiwata, and K. Kinosita, Jr. 1995. Unbinding force of a single motor molecule of muscle measured using optical tweezers. *Nature*. 377:251–254.
14. Mehta, A. D., J. T. Finer, and J. A. Spudich. 1997. Detection of single-molecule interactions using correlated thermal diffusion. *Proc. Natl. Acad. Sci. USA*. 94:7927–7931.
15. Lombardi, V., and G. Piazzesi. 1990. The contractile response during steady lengthening of stimulated frog muscle fibres. *J. Physiol*. 431: 141–171.
16. Finer, J. T., R. M. Simmons, and J. A. Spudich. 1994. Single myosin molecule mechanics: piconewton forces and nanometre steps. *Nature*. 368:113–119.
17. Molloy, J. E., J. E. Burns, J. Kendrick-Jones, R. T. Tregear, and D. C. White. 1995. Movement and force produced by a single myosin head. *Nature*. 378:209–212.
18. Dupuis, D. E., W. H. Guilford, J. Wu, and D. M. Warshaw. 1997. Actin filament mechanics in the laser trap. *J. Muscle Res. Cell Motil*. 18:17–30.
19. Greenleaf, W. J., M. T. Woodside, E. A. Abbondanzieri, and S. M. Block. 2005. Passive all-optical force clamp for high-resolution laser trapping. *Phys. Rev. Lett*. 95:208102.
20. Steffen, W., D. Smith, R. Simmons, and J. Sleep. 2001. Mapping the actin filament with myosin. *Proc. Natl. Acad. Sci. USA*. 98:14949–14954.
21. Steffen, W., D. Smith, and J. Sleep. 2003. The working stroke upon myosin-nucleotide complexes binding to actin. *Proc. Natl. Acad. Sci. USA*. 100:6434–6439.
22. Barclay, C. J. 1998. Estimation of cross-bridge stiffness from maximum thermodynamic efficiency. *J. Muscle Res. Cell Motil*. 19:855–864.
23. Lovell, S., T. Karr, and W. F. Harrington. 1988. Suppression of contractile force in muscle fibers by antibody to myosin subfragment 2. *Proc. Natl. Acad. Sci. USA*. 85:1849–1853.
24. Iwane, A. H., K. Kitamura, M. Tokunaga, and T. Yanagida. 1997. Myosin subfragment-1 is fully equipped with factors essential for motor function. *Biochem. Biophys. Res. Commun*. 230:76–80.
25. Veigel, C., J. E. Molloy, S. Schmitz, and J. Kendrick-Jones. 2003. Load-dependent kinetics of force production by smooth muscle myosin measured with optical tweezers. *Nat. Cell Biol*. 5:980–986.